Front. Struct. Civ. Eng. 2023, 17(2): 224–237
https://doi.org/10.1007/s11709-022-0914-1

RESEARCH ARTICLE

Numerical analysis of bearing behaviors of single batter piles under horizontal loads in various directions

Shuang ZHAO[a], Kuihua WANG[a*], Yuan TU[a], Weiqiu CHEN[b], Juntao WU[a]

[a] *College of Civil Engineering and Architecture, Zhejiang University, Hangzhou 310058, China*
[b] *School of Aeronautics and Astronautics, Zhejiang University, Hangzhou 310013, China*
[*] *Corresponding author. E-mail: zdwkh0618@zju.edu.cn*

ABSTRACT The horizontal bearing behavior of a single batter pile (SBP) is vital to its application in practical engineering; however, the horizontal responses of SBPs change with the directions of horizontal loads, and this phenomenon is rarely investigated. Therefore, the directional differences in the horizontal bearing behaviors of SBPs are investigated in this study. Four model tests are conducted to preliminarily examine the effects of the skew angle of horizontal loads on the horizontal bearing capacities and distributions of the bending moments of the SBPs. Subsequently, the differences in the responses of the SBPs under horizontal loads in various directions at full scale are analyzed comprehensively via finite-element (FE) analysis. The effects of the skew angle on SBP-soil interaction are discussed. Moreover, an empirical design method is proposed based on the FE analysis results to predict the bearing ratios of SBPs in medium-dense and dense sand while considering the effects of the skew angle, batter angle, and pile diameter. The method is confirmed to be effective, as confirmed by the close agreement between the predicting results with the model test (reported in this study) and centrifuge model test results (reported in the literature).

KEYWORDS single batter pile, skew horizontal load, model test, finite-element analysis, empirical design method

1 Introduction

Batter piles are extensively used to resist horizontal loads (e.g., wind, waves, and asymmetric earth pressure) in practical engineering (particularly in offshore engineering). It is generally believed that batter piles can transmit a portion of horizontal loads to axial loads to improve their horizontal bearing capacity [1,2]. However, owing to the unsatisfactory performance of batter piles during earthquakes, their application is not recommended in some codes [2]. In recent years, scholars have conducted centrifuge model tests and finite element (FE) modeling to investigate the seismic performance of batter piles and concluded that utilizing batter piles effectively reduced the displacement at the pile cap [3,4]; however, the distributions of internal forces in the batter piles were different from those in vertical piles [2,5–7]. This indicates that appropriately designed batter piles are beneficial to superstructures. Thus, a design method for the batter piles is urgently needed on the premise of understanding their bearing behaviors.

The bearing capacities and distributions of internal forces are important considerations when designing batter piles and have garnered extensive research interest [8–10], particularly the horizontal bearing behaviors of single batter piles (SBPs) [11–13]. Existing studies primarily focused on the horizontal bearing capacities of positive batter piles (PBPs) and negative batter piles (NBPs), which implies that the directions of the horizontal loads are parallel to PBPs or against NBPs the inclination of SBPs. Notably, 1g and centrifuge model tests are effective laboratory methods for comprehensively investigating the bearing behaviors of piles [1,14,15]. Meyerhof and Yalcin [16,17] conducted several model tests to investigate the effects of the layered condition, load inclination, and batter angle on the bearing capacities of SBPs. Rao and Veeresh [18] utilized 12 mm aluminum model piles of various lengths to investigate the horizontal bearing capacities of SBPs in clay. The results indicated that the horizontal bearing

Article history: Received Jun 8, 2022; Accepted Sep 25, 2022

capacity of SBPs increased as the batter angle increased from –30° to 30°. Zhang et al. [1] investigated the horizontal bearing capacities of SBPs in loose and medium-dense sand via centrifuge model tests and discovered that PBPs afforded higher bearing capacities. In recent years, the finite-element (FE) method has been used extensively to investigate the responses of single piles under lateral loads as it can effectively simulate soil behaviors and pile-soil interactions [19–21]. Cao and Fan [22] investigated the horizontal bearing capacities of SBPs via FE modeling and discovered that PBPs provided greater horizontal bearing capacity than vertical piles of the same material and size. Furthermore, modified p–y (soil resistance–deflection) curve methods for predicting the horizontal bearing capacities of PBPs and NBPs were proposed based on a three-dimensional wedge model, model tests, and a strain wedge model [23–25]. However, horizontal loads are not necessarily imposed in a fixed direction, particularly in ocean engineering, and the directions of wind and waves change in real time. Thus, the bearing behaviors of SBPs under horizontal loads in various directions should be investigated more comprehensively owing to their significance to engineering applications.

In this study, model tests and FE analyses were performed to investigate the directional differences in the horizontal bearing behaviors of SBPs. The main objectives of this study are as follows: 1) to preliminarily investigate the effects of the skew angle (δ) on the horizontal bearing behaviors of SBPs in sand through model tests; 2) to analyze the effects of parameters such as the skew angle, batter angle, relative density of sand, pile length, and diameter on the horizontal bearing capacities of SBPs; 3) to discuss the effects of δ on SBP-soil interactions; and 4) to propose a method for predicting the horizontal bearing ratios (β) of SBPs.

2 Description of model test

In this study, model tests were conducted to investigate the effects of the skew angle (δ) on the lateral bearing behaviors of SBPs and to verify the accuracy of FE models developed in this study. Both piles are assumed to be “wished-in-place” without considering the effects of pile installation [26]. The detailed configurations of the model tests are presented in the following subsections.

2.1 Horizontal loads in various directions

Figure 1 illustrates the batter angle (θ) and skew angle (δ). The θ of the SBP denotes the acute angle between the pile axis and vertical direction. Meanwhile, δ denotes the angle between the horizontal direction, which is against the inclination of the SBP, and the skew horizontal load; it ranges from 0° to 180°. In addition, an X–Y–Z rectangular coordinate system, as shown in Fig. 1, is introduced. The Z-axis is parallel to the pile axis, and the Y-axis is the projection of the lateral load on the plane, which is normal to the Z-axis. The origin is at the intersection of the pile axis and soil surface.

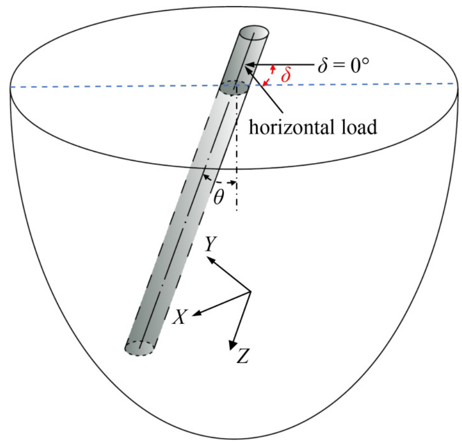

Fig. 1 Diagram showing SBP and skew horizontal load.

2.2 Soil condition

The soil used in the model test was dry silica sand with a mean particle size (d_{50}) of 0.20 mm, and it was classified as poorly graded sand [27]. The model tests were conducted in a 0.8 m × 0.8 m × 1.2 m chamber, and the thickness of the model ground was 1.0 m. To control the homogeneity of the model ground, the sand was prepared in five layers (each layer was approximately 0.20 m thick). Dry sand with a certain weight was spread evenly within the layers in the chamber. The sand in each layer was compacted using a plate vibrator until each layer was compacted to a determined depth. First, the sand beneath the pile toe was prepared. Subsequently, the model pile was placed in a fixture at the pile head. Thereafter, the sand surrounding the model pile was poured and compacted in layers, and the fixture was removed when the model pile stabilized. Notably, the pile inclination affected the homogeneity of the sand surrounding the piles, which is an important consideration.

2.3 Model pile

In this study, the length scale factor was approximately 1/20, based on the scaling law for a 1g model test [28]. The length (L) and outer diameter (D) of the model piles were approximately 60 and 5 cm, respectively, and the length-to-diameter ratio (L/D) was 12. Figure 2 shows the piles used in the model tests. The model piles were prepared using aluminum pipes with an outer diameter of 5.0 cm and a thickness of 1.0 mm. To intensify the pile-soil interaction, coarse sandpaper was used to roughen the outer surface of the aluminum pipes. As shown in Fig. 2, resistance strain gauges were attached onto the outer

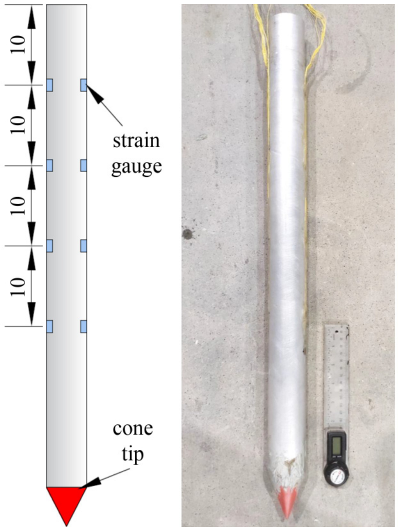

Fig. 2 Schematic illustration of the model piles (unit: cm).

surface of the aluminum pipes at specified positions and were shielded by epoxy resin. The resistance strain gauges measured 10 mm × 5 mm, and their resistance was 120 Ω. Additionally, the pile toe was sealed using a cone tip.

2.4 Static load test

Figure 3 shows a photograph of the equipment used in the static load test. As shown in Fig. 3, the equipment in the model test included a hydraulic jack, dial indicator, load cell, and data-acquisition instrument. The θ values of the piles considered in the model tests were 0° and 20°, whereas the δ values were 0°, 90°, and 180°. Figure 4 shows a schematic illustration of the static load test. The pile top was located 12 cm above the soil surface, and a horizontal load (H) was applied at a height of 8 cm. The horizontal distance from the lateral boundary of the chamber to the model pile exceeded $6D$ (30 cm), and the bottom of the chamber was located more than $10D$ away from the pile toe. The boundary effect was negligible in this model test configuration [21,29]. The horizontal load was imposed using a hydraulic jack and was measured using a load cell. The displacement at the loading position was measured using a dial indicator.

A multistage loading method was adopted for the loading process. The applied load, the displacement at the loading position, and the strains of the resistance strain gauges were recorded at each loading step.

3 Model test results

In this section, the model test results, including the load–displacement curves and the distributions of the pile bending moments, are presented below based on the effect of δ on the horizontal bearing behaviors of the SBPs.

3.1 Load−displacement response

The H–w curves of the SBPs under horizontal loads in various directions are presented in Fig. 5, where H and w denote the horizontal load and displacement in the loading direction, respectively. As shown in Fig. 5, the values of w increased with H, and the rate of increase augmented gradually. In the model tests, w increased as δ decreased under the same H. Consequently, an inflection point was not observed on the H–w curves, and the maximum measured horizontal displacement for the 20° SBP at δ = 180° was approximately 4.11 mm. Therefore, the horizontal bearing capacities (H_u and H_{u0}) of the pile were defined as w = 8%D (4 mm) in the model tests. Here, H_u and H_{u0} represent the horizontal bearing capacities of the SBP and corresponding vertical pile, respectively. The dashed line in Fig. 5 indicates the displacement level for determining the values of H_u for

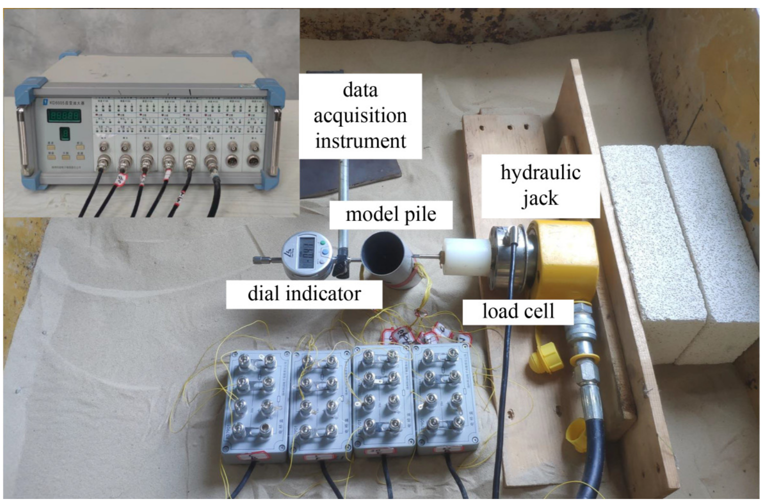

Fig. 3 Setup for the static load test.

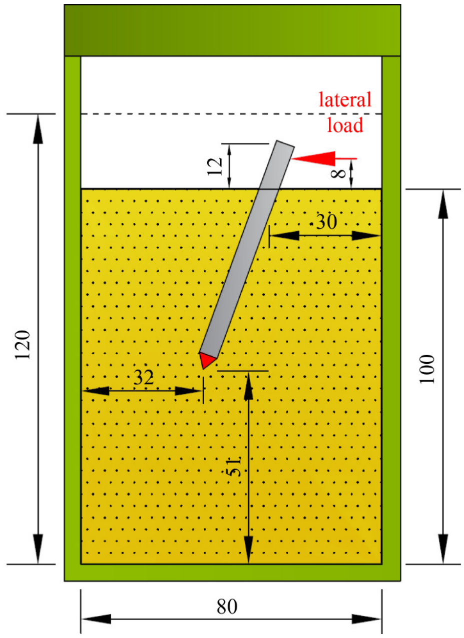

Fig. 4 Schematic illustration of static load test (unit: cm).

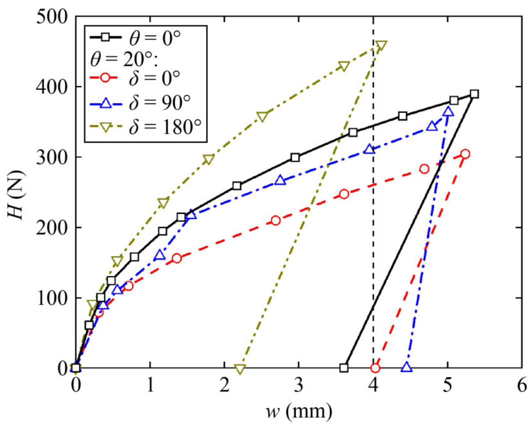

Fig. 5 H–w curves for SBPs in the model tests.

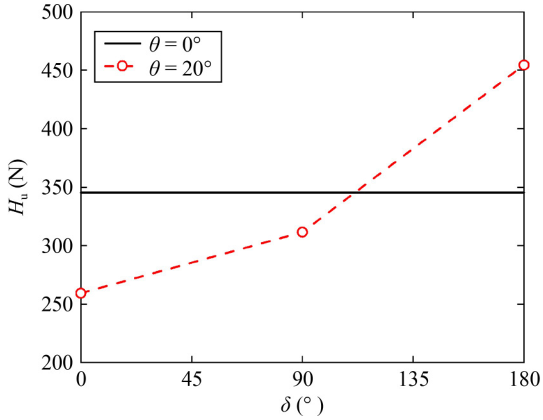

Fig. 6 Values of H_u for SBPs in the model tests.

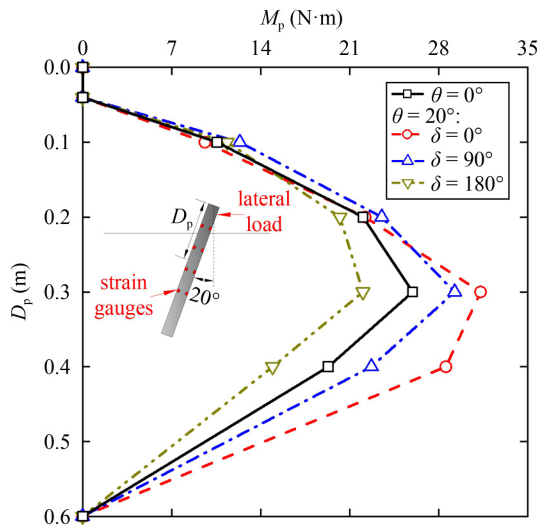

Fig. 7 Pile bending moment profiles for SBPs in the model tests under H = 150 N.

the SBPs. Figure 6 presents the values of H_u for the SBPs obtained from the model tests. The model test results indicate that the values of H_u for the SBPs increased with δ. In the model test, the horizontal bearing capacity of the vertical pile (H_{u0}) was 345.3 N. The values of H_u for the 20° SBP at δ = 0°, 90°, and 180° were 259.3, 311.5, and 454.5 N, respectively, which corresponded to 75.1%H_{u0}, 90.2%H_{u0}, and 131.6%H_{u0}, respectively. The δ of the SBPs for providing the same horizontal bearing capacity as the corresponding vertical pile was defined as δ_e, which was approximately 111° in the model test configuration.

3.2 Pile bending moment

Figure 7 presents the M_p–D_p curves for the SBPs under various δ, where M_p denotes pile bending moment and D_p denotes the length from the pile section to the pile top along the pile shaft. As shown in Fig. 7, in the model test, M_p first increased and then decreased as D_p increased. The maximum pile bending moment (M_{max}) appeared at approximately D_p = 0.3 m. These results demonstrate that, under the same lateral load, the pile bending moments decreased as the skew angle increased.

Figure 8 shows the M_{max} values obtained from the model test results. When H = 150 N, the values of M_{max} for the 20° SBP at δ = 0°, 90°, and 180° were 31.29, 29.26, and 22.05 N·m, respectively, which were 120.5%, 112.7%, and 84.9% of those for the vertical pile (25.96 N·m). M_{max} increased almost linearly as H increased. The slopes of the M_{max}–H curves decreased as δ increased, and the decreasing trend was particularly evident when 90° < δ < 180°.

4 Numerical simulation

To compensate for the limitation of the model test [30], FE analysis was performed to observe the bearing behaviors of the SBPs at full scale using the commercial finite element modeling (FEM) program ABAQUS. The model tests conducted in this study and the centrifuge model test of a single pile subjected to a lateral load [31] were first analyzed to examine the accuracy of the FE models. Subsequently, full-scale modeling was performed. All conditions considered in the full-scale model are presented in Table 1. Considering the wide application of concrete piles, the piles used in the full-scale modeling were simulated using a concrete material model. In addition, in the FE models, to mesh the pile and soil models more effectively, the horizontal sections of the piles were set as circular, where D denotes the diameter of the horizontal section. This simplification rendered the calculated lateral bearing capacities of the SBPs more conservative.

4.1 Finite element mesh

A diagram of a typical FE model is shown in Fig. 9. The meshes of the soil and pile were created separately, and C3D8R elements were used in both meshes. The sizes of the soil mesh, which were designed meticulous, decreased gradually along the direction near the pile mesh. The lateral distance between the lateral boundary of the model and pile exceeded 15D. The bottom of the model was 10D away from the pile toe. The piles were "wished-in-place," which indicates that the piles were located in the pre-bored holes in the soil mesh. The sides

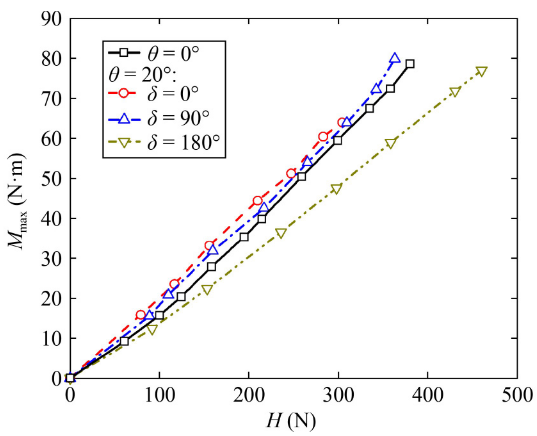

Fig. 8 M_{max}–H curves for SBPs in the model tests.

Table 1 Detailed simulation conditions for the full-scale modeling

parameter	value
pile length, L (m)	15, 25, 40
horizontal section diameter, D (m)	0.5, 1.0, 1.5
relative density of sand, D_r (%)	50%, 80%
batter angle, θ (°)	0, 10, 15, 20, 25
skew angle, δ (°)	0, 30, 60, 90, 120, 150, 180

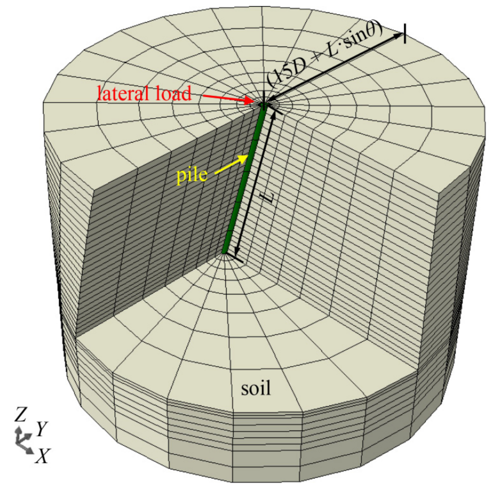

Fig. 9 FE model used in current study.

of the soil resisted against normal movements, and the bottom of the soil was fully constrained. The pile was fully embedded in the soil, and lateral loads were applied to the pile top in the form of a concentrated force.

4.2 Constitutive models and parameters

The horizontal responses of the piles were nonlinear because the mechanical behaviors of the concrete pile, soil, and pile-soil interaction were all nonlinear. Therefore, the appropriate nonlinear elastoplastic constitutive models must be adopted to simulate these mechanical behaviors.

4.2.1 Concrete model

The concrete smeared crack (CSC) model was adopted to simulate the mechanical behaviors of concrete piles in the FE modeling [32]. In the CSC model, the linear elastic model was adopted to describe the elastic behavior of the concrete before cracking, and the reversible concrete response after cracking was described based on oriented damaged elasticity concepts [33]. The elastoplastic behavior of the CSC was governed using an isotropic hardening yield surface function, and the cracking point was predicted using a crack-detection surface function [32]. The elastic modulus of the concrete pile (E_c) was 30 GPa, and the failure stress was 37.92 MPa. In addition, uniform reinforcements (steel in concrete piles) were considered. The longitudinal reinforcement ratio was approximately 0.8%. Reinforcements in the piles were realized using embedded shell elements (S4R), as illustrated in Fig. 10. Steel rebars were embedded in the concrete elements.

4.2.2 Sand model

An elastoplastic material was used to simulate the actual properties of sand, and the Mohr–Coulomb failure criterion with a non-associated flow rule was adopted to describe the plastic failure of the sand. The elastic modulus of sand is stress dependent, as shown by the following equation [34]:

$$E_s = \kappa \cdot \sigma_{at} \cdot \left(\frac{\sigma_m}{\sigma_{at}}\right)^{\lambda}, \tag{1}$$

where σ_{at} is the atmospheric pressure (101 kPa); σ_m is the mean principal stress; κ and λ are material stiffness constants, which were determined based on values recommended in Refs. [34,35]. Because batter piles are deep foundations that are widely used in offshore engineering, the sand in full-scale modeling was saturated, and the submerged unit weight was adopted. The accumulation of pore water pressure was not considered. The parameters of the sand used in the full-scale modeling are listed in Table 2.

4.2.3 Batter pile-soil interaction

To consider the separation and relative movement between the SBP and soil, the interaction between the SBP and sand was modeled via the Coulomb model, the SBP-soil friction increased linearly with the normal pressure. The contact friction angle of the Coulomb model was 0.67ϕ [34,35], and SBP-soil separation was allowed when the SBP-soil contact pressure was 0 or the relative SBP-soil movement reached the maximum allowable elastic slippage.

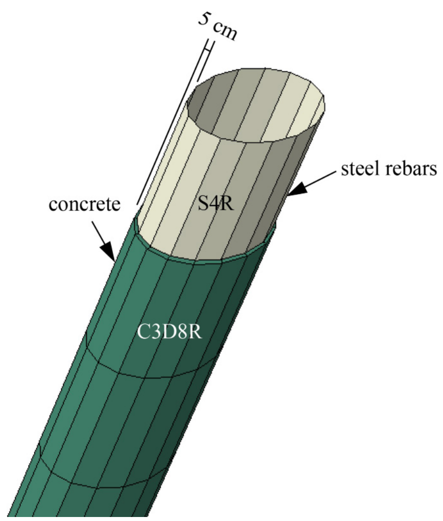

Fig. 10 Details of reinforcements in the piles illustrated using embedded shell elements.

4.3 Calculation procedures

In the current study, the piles were “wished-in-place”, and the installation effect was not considered. The following three procedures were performed in the numerical analysis.

1) Applying gravity and a predefined stress field to the model; the latter was added to balance the gravitational force to achieve the initial geostatic equilibrium state.

2) Activating the interaction between the SBP and sand.

3) Imposing a horizontal load at the pile top in the form of concentrated force until the displacement at the pile top in the loading direction reached 12%D.

4.4 Validation of the finite element models

4.4.1 Case 1: Model test

First, the model tests conducted in this study were simulated. To obtain a high-quality mesh and improve the convergence of the FE models, the piles were modeled as solids with an equivalent horizontal section flexural stiffness. The soil parameters are presented in Table 3. In the model-scale modeling, the depth of the soil was set as only 1 m; therefore, the elastic modulus of the sand was set as a constant. Figure 11 shows a comparison of the H–w curves obtained from the model tests and FEM results, and good agreement was observed between them. Additionally, the results verified that simplifying the horizontal sections of the piles as circular did not significantly affect the calculation results.

4.4.2 Case 2: Centrifuge model test

A centrifuge model test of a single pile subjected to a

Table 2 Default parameters of sand used in modeling

soil	unit weight γ_s' (kN/m^3)	material parameters		Poisson’s ratio υ	internal friction angle ϕ (°)	dilation angle ψ (°)	cohesion c (kPa)
		λ	κ				
medium-dense sand (D_r = 50%)	11	600	0.6	0.25	35.0	5.0	0.1
dense sand (D_r = 80%)	11	1000	0.5	0.25	37.5	7.5	0.1

Table 3 Default parameters of sand in the model-scale modeling

soil	unit weight (kN/m^3)	elastic modulus E_p (MPa)	Poisson’s ratio υ	internal friction angle ϕ (°)	dilation angle ψ (°)	cohesion c (kPa)
sand	15.386	17.0	0.3	34.1	0	0.34

lateral load reported in Ref. [31] was used to verify the accuracy of the FE models developed in this study. The soil parameters are presented in Table 4. The diameter and length of the pile were 2.5 and 65 m, respectively. The embedded depth of the pile was 50 m, and the load was applied at a height 6.75 m above the soil surface. Figure 12 shows a comparison of the H–w curves obtained from the centrifuge model test and FEM results. The H–w curve obtained from the FEM results was consistent with the centrifuge model test results. This implies that the FE models developed in this study can accurately simulate the horizontal bearing behavior of single pile.

4.5 Finite element results

In full-scale modeling, the bearing capacity of the SBP (H_u) is defined as the displacement when the pile top reaches 0.1D. Figure 13 presents the typical H_u–δ curves for the SBPs in medium-dense sand obtained from the full-scale modeling results. Similar to the model test results, the results in Fig. 13 indicate that the values of H_u increased with δ, and that the increasing rate presented a "slow–rapid–slow" trend. The results show that the values of δ_e increased with θ and were 100°–115°.

Figure 14 shows the distribution of the pile bending moments along the pile shaft under the simulation conditions shown in Fig. 14 when H = 600 kN. The results in Fig. 14 show that pile bending occurred primarily in the upper 12D of the SBPs, and that the values of M_p increased first and then decreased in this section. In addition, slight reverse bending was observed in the deeper sections of the SBPs. The maximum bending moment of the vertical pile was similar to that of the 15° SBP when δ = 90°; however, it occurred in a shallower pile section.

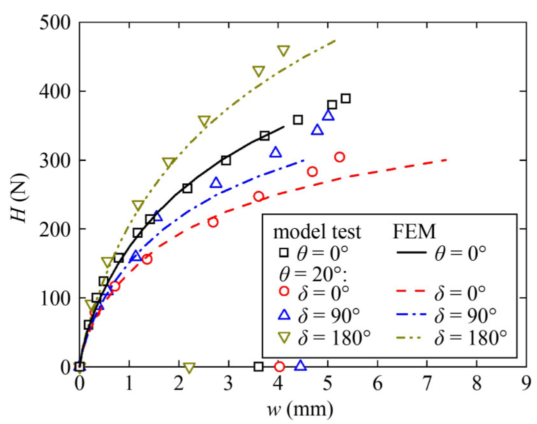

Fig. 11 Comparison of H–w curves of piles obtained from model tests and FEM results.

Table 4 Default parameters of sand used in centrifuge model test [36]

soil	unit weight γ_s' (kN/m^3)	material parameters λ	material parameters κ	Poisson's ratio υ	internal friction angle ϕ (°)	dilation angle ψ (°)	cohesion c (kPa)
sand	9.45	560	0.6	0.21	34.8	2.9	0.1

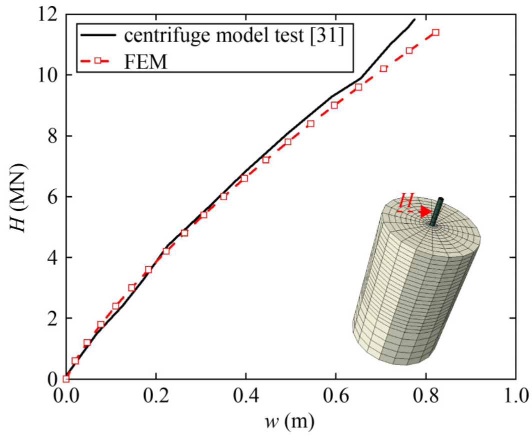

Fig. 12 Comparison of H–w curves for piles obtained from centrifuge model test and FEM results.

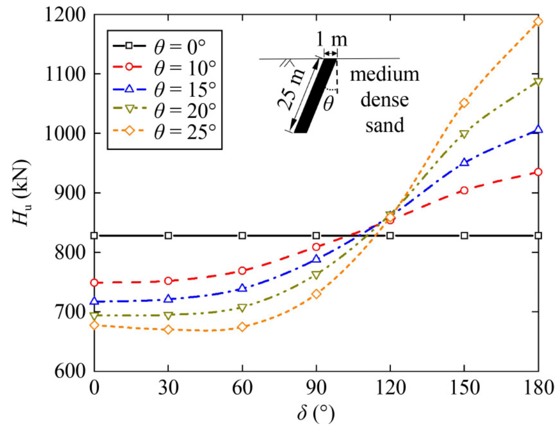

Fig. 13 Typical H_u–δ curves of SBPs in full-scale modeling.

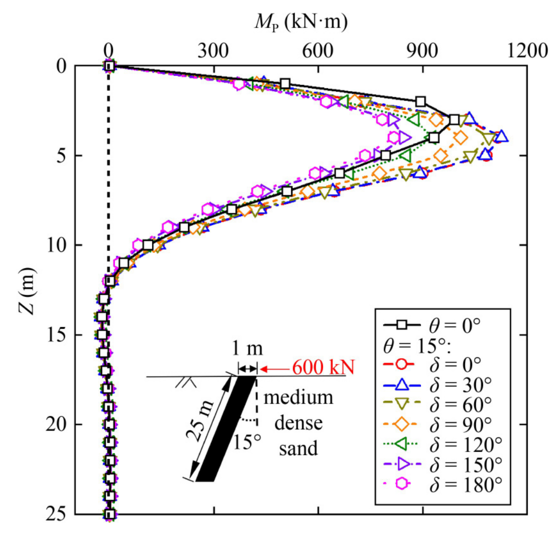

Fig. 14 Distribution of M_p vs. Z based on H = 600 kN.

5 Analysis and discussion

In this section, the effects of the relative density of sand (D_r) and the design parameters of the pile on the horizontal bearing capacities (H_u) of the SBPs are discussed. Additionally, the interactions between the SBPs and soil are discussed to provide a deeper understanding regarding the effects of δ on the horizontal bearing behavior of the SBPs.

5.1 Effect of the relative density of sand

D_r, which governs the soil parameters (such as ϕ, E_s, and ψ), significantly affects the bearing capacity of single piles [37]. Thus, a comparison of the horizontal bearing capacities of the SBPs in sand with various D_r values (D_r = 50% and 80%) is presented in this section. To show the results more clearly, β is introduced, as follows [30]:

$$\frac{H_u}{H_{u0}} = \beta. \tag{2}$$

The results of β for SBPs in sand with various D_r values are presented in Fig. 15. Based on Fig. 15, the trends of β vs. δ were not affected by the change in D_r. β increased with δ, and the increasing rates show the "slow−rapid−slow" trend. As D_r increased, the increase rates of β at the same δ increased, but the values of δ_e decreased slightly.

5.2 Effect of pile length and diameter

Length (L) and diameter (D) are both significant design parameters for piles. Therefore, the effects of L and D on the β of the SBPs are analyzed in this section. Typical β–δ curves for SBPs of various L and D are presented in Figs. 16(a) and 16(b), respectively. As shown in Fig. 16(a), the variation in L barely affected the β–δ curves. The horizontal bearing behaviors of the single piles were unaffected by the pile length when the embedded depth exceeded the critical length (L_{cr}) [36,38]. Considering that the designed embedded depth of the pile is generally greater than L_{cr} to ensure the safe service of the pile foundation, the effects of L on β is negligible in practical

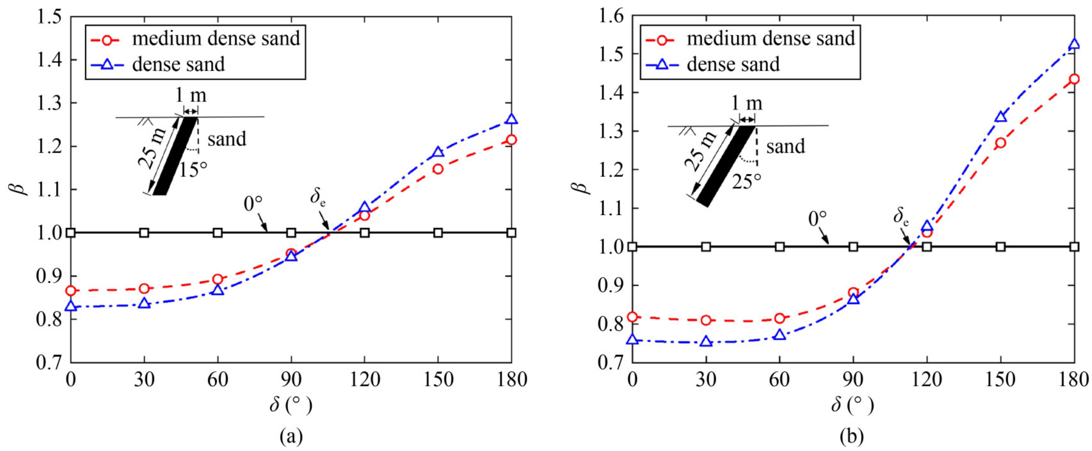

Fig. 15 β–δ curves of SBPs in sand of various relative densities: (a) θ = 15°; (b) θ = 25°.

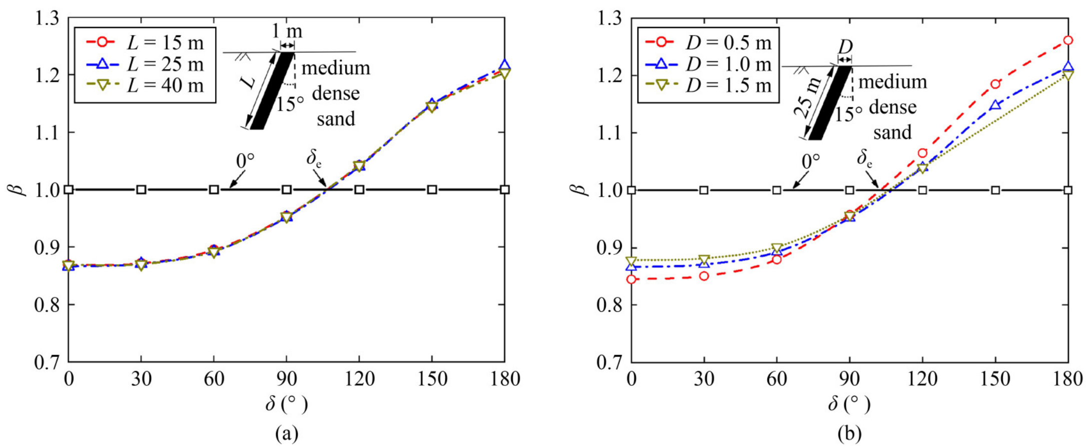

Fig. 16 β–δ curves of SBPs of various lengths and diameters in medium-dense sand: (a) various pile lengths; (b) various pile diameters (The FE model for 15° SBP at D = 1.5 m and δ = 150° was not convergent when w = 0.1D).

engineering. In addition, Fig. 16(b) shows that the variation in D primarily affected the increasing rate of β with δ. As D increased, the rate of increase of β at the same δ decreased, and the values of δ_e increased slightly. These results indicate that increasing D can reduce the effect of δ on the β of the SBPs to some degree.

5.3 Discussion regarding batter pile-soil interaction

In existing studies, piles are generally modeled as a beam on a nonlinear Winker foundation [23–25], whereas soil is simplified as a series of nonlinear springs (p–y curves). Therefore, in this section, the normal deflection (y) profiles, soil resistance (p) profiles, and p–y curves for shallow soil are compared to investigate the effects of δ on SBP-soil interaction.

Figure 17 shows the distributions of y vs. Z for the 15° SBP and vertical pile under 600 kN horizontal loads obtained from the FEM results. The maximum deflection appeared at the pile top because the latter was unconstrained and decreased rapidly along the pile shaft. The normal deflection was primarily concentrated in the upper 8D of the SBPs, and the values of y at the same Z increased as δ decreased from 180° to 0°, particularly when 60° < δ < 150°. The maximum deflection of the 15° SBP at δ = 0°, 30°, 60°, 90°, 120°, 150°, and 180° were 149.3%, 144.1%, 133.4%, 114.7%, 92.6%, 77.4%, and 71.5% that of the vertical pile.

The soil resistance profiles were obtained by differentiating the fitting functions of the shear force-Z curves [39]. Figure 18 shows the distribution of the soil resistance profiles for the 15° SBP and vertical pile under 600 kN horizontal loads. Based on the distributions of p vs. Z, the pile was categorized into the following three sections: I. Main deflection section (p > 0); II. reverse bending section (p < 0); III. static sections (p = 0). In the main deflection section, the soil resistance first increased and then decreased after reaching the peak value. Before reaching the peak value, the p values at the same Z increased with δ. However, the decreasing rate along the Z of p decreased as δ increased after reaching the peak value. Although only slight reverse bending was observed from the distribution of the pile normal deflection (Fig. 17), distinct reverse bending was observed from the distribution of soil resistance (Fig. 18). The lengths of the main deflection section (L_m) and reverse bending section (L_r) were approximately 6.8D and 9.2D, respectively. L_m and L_r decreased slightly as δ increased.

Figure 19 shows the p–y curves for the 15° SBP and vertical pile at Z = 1D, 2D, and 3D. As shown in Fig. 19, the soil resistances first increased rapidly, and as the increasing rate decreased, the soil resistances stabilized. Furthermore, the soil resistances at the same pile deflection increased with Z, as well as when δ increased from 0° to 180°; the increasing rate exhibited a "slow–rapid–slow" trend as δ increased. When y = 0.07 m, the soil resistance at Z = 1D for the 15° SBP at δ = 0°, 30°, 60°, 90°, 120°, 150°, and 180° were 69.0%, 72.2%, 77.0%, 86.5%, 101.7%, 116.6%, and 129.0% that of the vertical pile, respectively. A higher shallow soil resistance at the same pile deflection allowed the SBP at a greater δ to provide a larger horizontal bearing capacity. The shallow soil can provide less horizontal stiffness when δ is relatively small; thus, deeper sections must be activated in the pile to resist horizontal loads. This entails an increase in both L_m and L_r as δ decreases.

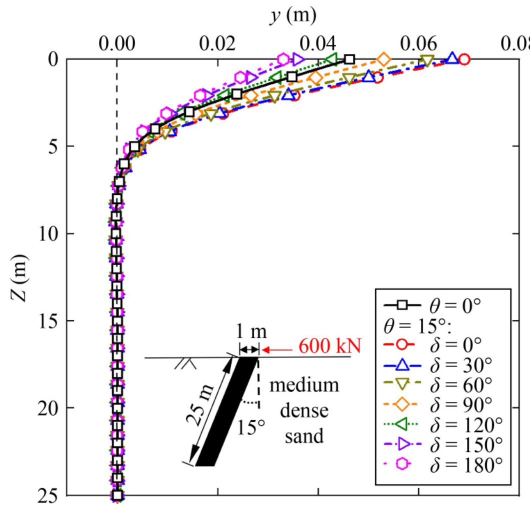

Fig. 17 Distributions of normal deflection (y) vs. Z for 15° SBP and vertical pile under 600 kN horizontal loads.

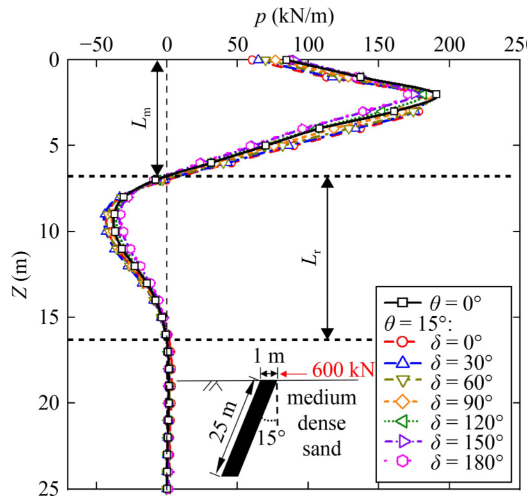

Fig. 18 Distributions of p vs. Z for 15° SBP and vertical pile under H = 600 kN.

6 Prediction method for single batter piles

The effects of θ and δ on the relationship between H_u and H_{u0} are reflected by β. Based on the analysis presented in

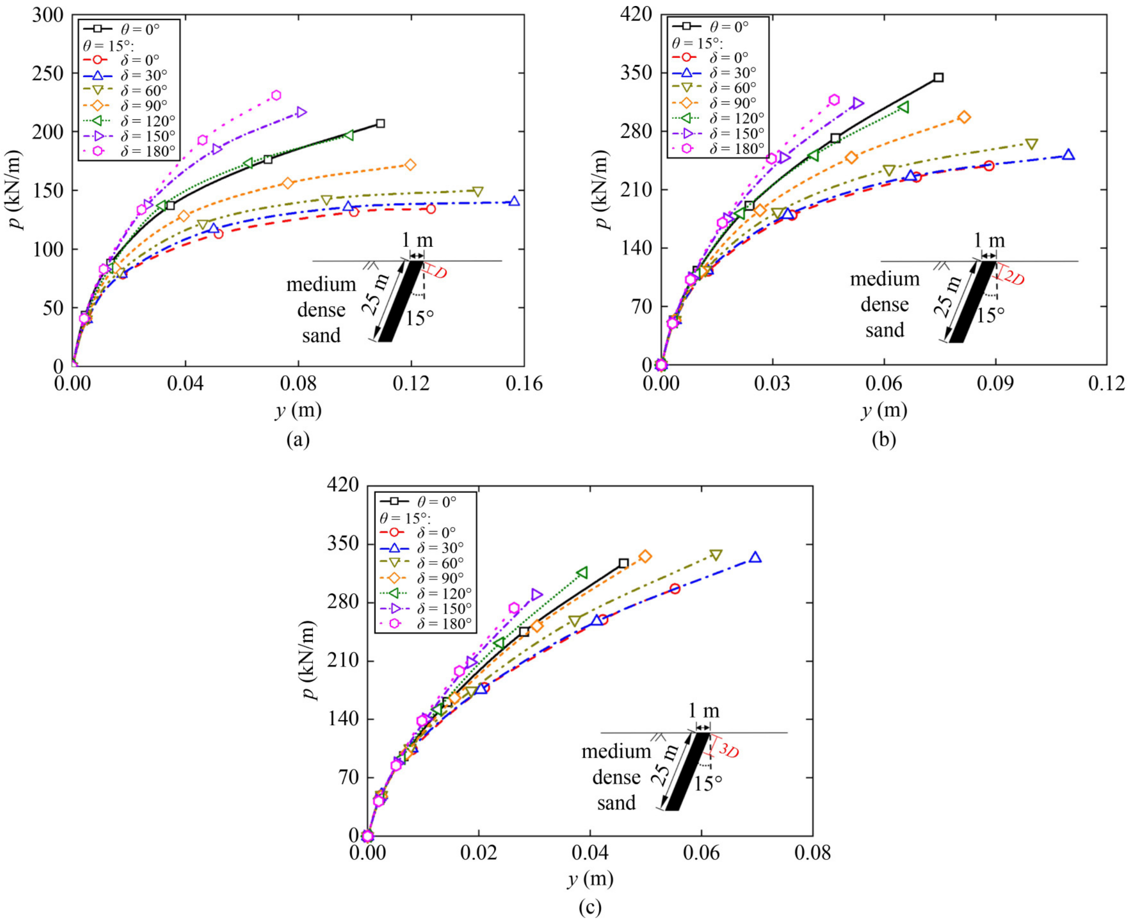

Fig. 19 p–y curves for 15° SBP and vertical pile: (a) $Z = 1D$; (b) $Z = 2D$; (c) $Z = 3D$.

the previous section, β is primarily affected by δ, θ, D_r, and D.

First, the relationship between β and δ is analyzed. Figure 20 shows the typical values of β for various δ values obtained from the FEM results. A power model is used to describe the relationship between β and δ, as follows:

$$\beta = a \cdot \left(\frac{\delta}{180}\right)^b + c, \tag{3}$$

where a, b, and c are the functions of θ, D_r, and D, respectively. To use the power model, δ is set to 0.001 when its actual value is 0. The results in Fig. 20 show that the power model can capture the relationship between β and δ.

Next, the relationships among a, b, c, and θ are analyzed. Figure 21 shows the typical results of a, b, and c for various θ values obtained from the FEM results. The results shows that a, b, and c varied linearly with the increase in θ, and that the slopes of the a–θ, b–θ, and c–θ curves varied with D_r. Linear functions were adopted to capture the relationship between θ and each of a, b, and c, as follows:

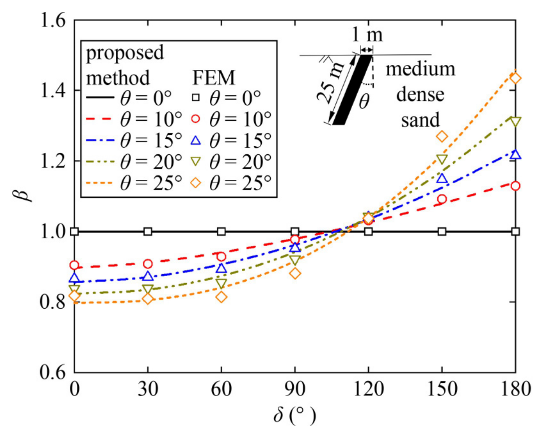

Fig. 20 β vs. δ.

$$a = k \cdot \frac{\theta}{90}, \tag{4}$$

$$b = m \cdot \frac{\theta}{90} + 1, \tag{5}$$

$$c = n \cdot \frac{\theta}{90} + 1, \tag{6}$$

where k, m, and n are the slopes of the a–$\left(\frac{\theta}{90}\right)$, b–$\left(\frac{\theta}{90}\right)$, and c–$\left(\frac{\theta}{90}\right)$ curves, respectively, and both sets of parameters are functions of D_r.

To conveniently describe the relationships between D_r and each of k, m, and n, normalized parameters ($k_c/k_{50\%}$, $m_c/m_{50\%}$, and $n_c/n_{50\%}$) are introduced, where k_c, m_c, and n_c denote the values of k, m, and n for D_r = c, respectively. The normalized parameter values for D_r = 50% and 80% are shown in Fig. 22. Similarly, linear functions are used to describe the relationships between D_r and each of $k_c/k_{50\%}$, $m_c/m_{50\%}$, and $n_c/n_{50\%}$, as follows:

$$\frac{k_c}{k_{50\%}} = 0.86 \times D_r + 0.57, \tag{7}$$

$$\frac{m_c}{m_{50\%}} = -0.36 \times D_r + 1.18, \tag{8}$$

$$\frac{n_c}{n_{50\%}} = 0.94 \times D_r + 0.53. \tag{9}$$

In addition, a, b, and c are functions of D. Normalized parameters (a_d/a_1, b_d/b_1, and c_d/c_1) are introduced, where a_d, b_d, and c_d are the values of a, b, and c, respectively, for D = d. Figure 23 shows the typical values of a_d/a_1, b_d/b_1, and c_d/c_1 vs. D. Combining these values with the results shown in Fig. 23, the correlations of a_d/a_1, b_d/b_1, and c_d/c_1 with D can be expressed as follows:

$$\frac{a_d}{a_1} = -0.278 \times \ln D + 1, \tag{10}$$

$$\frac{b_d}{b_1} = 0.0842 \times \ln D + 1, \tag{11}$$

$$\frac{c_d}{c_1} = 0.0418 \times \ln D + 1. \tag{12}$$

Based on the analysis above, the β of the SBPs can be predicted as follows:

$$\begin{aligned}\beta = {} & (-0.278 \times \ln D + 1)\left[(0.86 \times D_r + 0.57) \times k_{50\%} \cdot \frac{\theta}{90}\right] \\ & \cdot \left(\frac{\delta}{180}\right)^{(0.0842\times\ln D+1)[(-0.36\times D_r+1.18)\times m_{50\%}\cdot\frac{\theta}{90}+1]} \\ & + (0.0418 \times \ln D + 1) \cdot \left[(0.94 \times D_r + 0.53) \times n_{50\%} \cdot \frac{\theta}{90} + 1\right],\end{aligned} \tag{13}$$

where the values of $k_{50\%}$, $m_{50\%}$, and $n_{50\%}$ are 2.3183, 5.1396 and –0.7859, respectively. The FEM results were verified using Eq. (13), and the comparison results are shown in Fig. 24. The results yielded by the proposed method agreed well with the FEM results because the effects of δ, θ, D_r, and D were considered. Furthermore, the model test results and centrifuge model test results from Ref. [1] were used to examine the accuracy of the

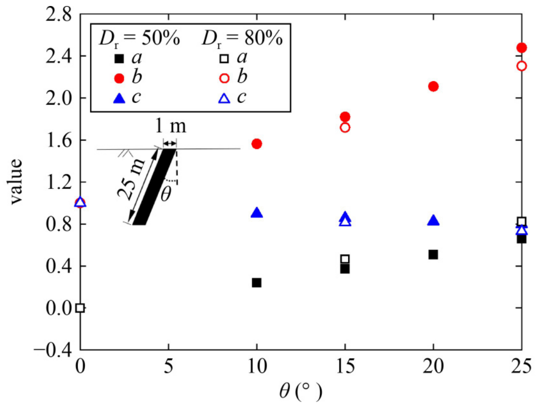

Fig. 21 Values of a, b, and c for sand of various relative densities.

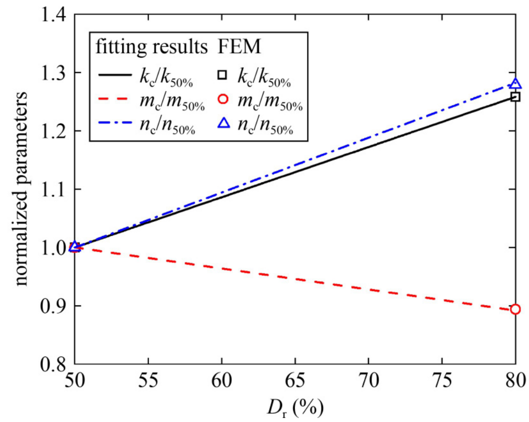

Fig. 22 Values of normalized parameters ($k_c/k_{50\%}$, $m_c/m_{50\%}$, and $n_c/n_{50\%}$) vs. D_r.

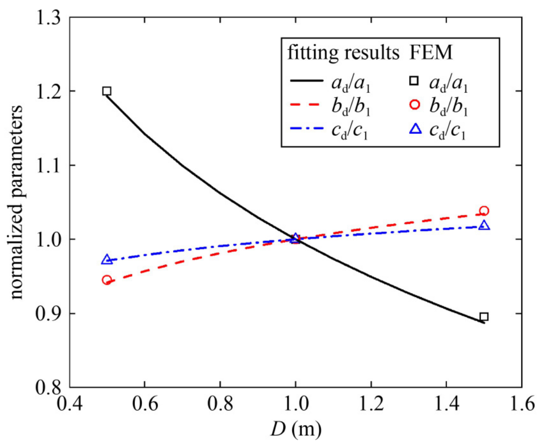

Fig. 23 Values of normalized parameters (a_d/a_1, b_d/b_1, and c_d/c_1) vs. D.

empirical design method, and the comparison results are presented in Figs. 25(a) and 25(b). Square piles were used in the centrifuge model test [1]; therefore, the diameter of the piles was determined based on the equivalent horizontal section flexural stiffness. The results in Fig. 25(a) show that this method accurately predicted the variation in β vs. δ for the SBPs in the model tests, and the differences were attributable to scale effects. In addition, based on Fig. 25(b), the differences between the results yielded by the proposed method and the centrifuge model test results [1] were attributable to two aspects. 1) In the centrifuge model test, the piles were jacked into the sand; however, the piles considered in this study were "wished-in-place," and the effects of pile installation were not considered. 2) The piles used in the centrifuge model tests were aluminum piles; however, the piles considered in the current study were concrete piles with steel reinforcement and might crack during loading. Hence, the proposed method can be used to predict the β of SBPs in medium-dense and dense sand.

7 Conclusions

In this study, model tests and FE analysis were conducted to investigate the directional differences in the horizontal bearing behaviors of SBPs in sand. Based on the model test and FE analysis results, the following conclusions were inferred.

1) The H_u of the SBPs increased as δ increased from 0° to 180°, and the increasing rate presented a "slow−rapid−slow" trend. Meanwhile, the θ for the SBPs provided the same H_u as the vertical piles increased with θ from 100°–115°.

2) Under the same lateral load, the M_p at the same depth along the pile shaft increased as δ decreased. M_{max}

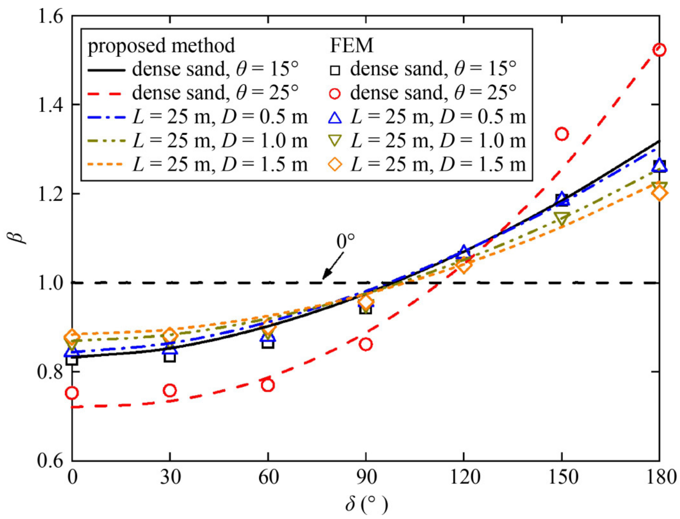

Fig. 24 β values for SBPs yielded by proposed method and obtained from FEM results.

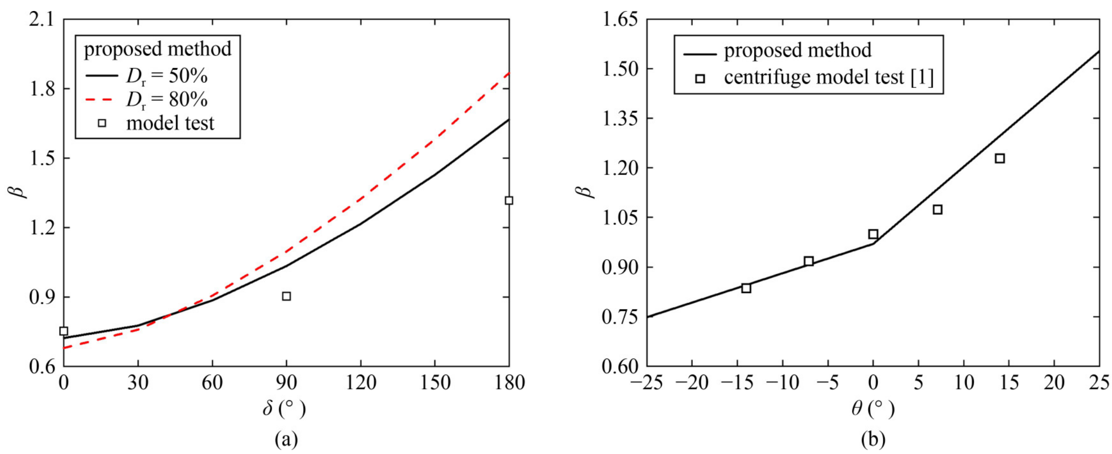

Fig. 25 β values for SBPs yielded by the proposed method and obtained from model test results: (a) model tests; (b) centrifuge model test [1].

increased almost linearly with H, and the slopes of the M_{max}–H curves decreased as δ increased.

3) As θ and D_r increased, the growth rate of β at the same δ increased. This was similarly observed as D decreased. The effect of L on β in SBPs used in practical engineering is negligible.

4) The shallow soil resistances at the same pile deflection increased with δ, which resulted in SBPs at larger δ values providing greater horizontal bearing capacity. In addition, the SBPs at smaller δ values required the activation of deeper pile sections to resist horizontal loads; therefore, greater deflections were generated in the upper sections.

5) Based on the FEM results, an empirical design method was proposed to analyze the values of β for SBPs embedded in medium-dense and dense sand under horizontal loads in various directions. The estimated results agreed well with the model test results and centrifuge model test results from the literature.

Acknowledgements This study was supported by the National Natural Science Foundation of China (Grant Nos. 52178358, 52108349, and 51779217) and the Key Project of the Natural Science Foundation of Zhejiang Province (No. LXZ22E080001).

References

1. Zhang L, Mcvay M C, Lai P W. Centrifuge modelling of laterally loaded single battered piles in sands. Canadian Geotechnical Journal, 1999, 36(6): 1074−1084
2. Giannakou A, Gerolymos N, Gazetas G, Tazoh T, Anastasopoulos I. Seismic behavior of batter piles: Elastic response. Journal of Geotechnical and Geoenvironmental Engineering, 2010, 136(9): 1187−1199
3. Bharathi M, Dubey R N, Shukla S K. Experimental investigation of vertical and batter pile groups subjected to dynamic loads. Soil Dynamics and Earthquake Engineering, 2019, 116: 107−119
4. Subramanian R M, Boominathan A. Dynamic experimental studies on lateral behaviour of batter piles in soft clay. International Journal of Geotechnical Engineering, 2016, 10(4): 317−327
5. Li Z, Escoffier S, Kotronis P. Centrifuge modeling of batter pile foundations under earthquake excitation. Soil Dynamics and Earthquake Engineering, 2016, 88: 176−190
6. Li Z, Escoffier S, Kotronis P. Centrifuge modeling of batter pile foundations under sinusoidal dynamic excitation. Bulletin of Earthquake Engineering, 2016, 14(3): 673−697
7. Sarkar R, Roy N, Serawat A. A three dimensional comparative study of seismic behaviour of vertical and batter pile groups. Geotechnical and Geological Engineering, 2017, 36(2): 763−781
8. Al-Neami A M, Rahil H F, Al-Bayati S K. Bearing capacity of batter piles embedded in sandy soil. International Journal of Geotechnical Engineering, 2016, 10(5): 529−532
9. Liu K, Han C, Xu C, Nie Z. Experimental study on deformation and load transfer mechanisms of symmetrical batter piles under vertical loading. Applied Sciences (Basel, Switzerland), 2021, 11(7): 3169
10. Kim J, Yun S K, Kang M, Kang G. Behavior characteristics of single batter pile under vertical load. Applied Sciences (Basel, Switzerland), 2021, 11(10): 1−18
11. Bajaj P, Yadu L, Chouksey S K. Behavior of vertical and batter piles under lateral, uplift and combined loads in non-cohesive soil. Innovative Infrastructure Solutions, 2019, 4(1): 1−17
12. Vu A T, Matsumoto T, Kobayashi S I, Nguyen T L. Model load tests on battered pile foundations and finite-element analysis. International Journal of Physical Modelling in Geotechnics, 2018, 18(1): 33−54
13. Xie Y, Liu C, Gao S, Tang J, Chen Y. Lateral load bearing capacity of offshore high-piled wharf with batter piles. Ocean Engineering, 2017, 142: 377−387
14. Baca M, Rybak J. Pile base and shaft capacity under various types of loading. Applied Sciences (Basel, Switzerland), 2021, 11(8): 1−15
15. Baca M, Brzakała W, Rybak J. Bi-directional static load tests of pile models. Applied Sciences (Basel, Switzerland), 2020, 10(16): 1−13
16. Meyerhof G G, Yalcin A S. Behaviour of flexible batter piles under inclined loads in layered soil. Canadian Geotechnical Journal, 1993, 30(2): 247−256
17. Meyerhof G G, Yalcin A S. Bearing capacity of flexible batter piles under eccentric and inclined loads in layered soil. Canadian Geotechnical Journal, 1994, 31(4): 583−590
18. Rao S N, Veeresh C. Influence of pile inclination on the lateral capacity of batter piles in clay. In: Proceeding of 4th International Offshore and Polar Engineering Conference. Golden, CO: ISOPE, 1994, 498−503
19. Li Z, Kotronis P, Escoffier S. Numerical study of the 3D failure envelope of a single pile in sand. Computers and Geotechnics, 2014, 62: 11−26
20. Wang A, Zhang D, Deng Y. Lateral response of single piles in cement-improved soil: Numerical and theoretical investigation. Computers and Geotechnics, 2018, 102: 164−178
21. Dong J, Chen F, Zhou M, Zhou X. Numerical analysis of the boundary effect in model tests for single pile under lateral load. Bulletin of Engineering Geology and the Environment, 2018, 77(3): 1057−1068
22. Cao W P, Fan W F. Numerical analysis on bearing and deformation behavior of horizontally loaded batter piles. China Journal of Highway and Transport, 2017, 30(9): 34−43 (in Chinese)
23. Ling D S, Ren T, Wang Y G. A *p*–*y* curves method for horizontal bearing characteristics of single batter pile in sands. Rock and Soil Mechanics, 2013, 34(1): 155−162 (in Chinese)
24. Cao W P, Xia B, Zhao M, Geo X. *P*–*y* curves of laterally loaded batter piles in sand and its application. Chinese Journal of Rock Mechanics and Engineering, 2018, 37(3): 743−753 (in Chinese)
25. Ashour M, Alaaeldin A, Arab M G. Laterally loaded battered piles in sandy soils. Journal of Geotechnical and Geoenvironmental Engineering, 2020, 146(1): 06019017
26. Fan S, Bienen B, Randolph M F. Centrifuge study on effect of installation method on lateral response of monopiles in sand. International Journal of Physical Modelling in Geotechnics, 2021,

21(1): 40−52
27. ASTM. Standard Practice for Classification of Soils for Engineering Purposes (Unified Soil Classification System). West Conshohocken, PA: ASTM International, 2010
28. Wood D M, Crewe A, Taylor C. Shaking table testing of geotechnical models. International Journal of Physical Modelling in Geotechnics, 2002, 2(1): 1−13
29. Zhu B, Xiong G, Liu J C, Sun Y X, Chen R P. Centrifuge modeling of a large-diameter single pile under lateral loads in sand. Chinese Journal of Geotechnical Engineering, 2013, 35(10): 1807−1815 (in Chinese)
30. Kyung D, Lee J. Interpretative analysis of lateral load-carrying behavior and design model for inclined single and group micropiles. Journal of Geotechnical and Geoenvironmental Engineering, 2018, 144(1): 04017105
31. Zhu B, Li T, Xiong G, Liu J. Centrifuge model tests on laterally loaded piles in sand. International Journal of Physical Modelling in Geotechnics, 2016, 16(4): 160−172
32. Hibbitt K. ABAQUS User's Manual, Version 6.8.2. 2008
33. Chen L, Fang Q, Huan Y, Zhang Y. Analysis on static performances of smeared cracking model for concrete in ABAQUS. Journal of PLA University of Science and Technology, 2007, 8(5): 478−485
34. Achmus M, Kuo Y S, Abdel-Rahman K. Behavior of monopile foundations under cyclic lateral load. Computers and Geotechnics, 2009, 36(5): 725−735
35. Kuo Y S, Achmus M, Abdel-Rahman K. Estimation of lateral deformation of monopile foundations by use of cyclic triaxial tests. Chinese Journal of Geotechnical Engineering, 2009, 31(11): 1729–1734 (in Chinese)
36. Liu J C, Xiong G, Zhu B, Ying P P. Bearing capacity and deflection behaviors of large diameter monopile foundations in sand seabed. Rock and Soil Mechanics, 2015, 36(2): 591–599 (in Chinese)
37. Li L, Zheng M, Liu X, Wu W B, Liu H, El Naggar M H, Jiang G. Numerical analysis of the cyclic loading behavior of monopile and hybrid pile foundation. Computers and Geotechnics, 2022, 144: 104635
38. Randolph M F. The response of flexible piles to lateral loading. Geotechnique, 1981, 31(2): 247−259
39. Ilyas T, Leung C, Chow Y, Budi S. Centrifuge model study of laterally loaded pile groups in clay. Journal of Geotechnical and Geoenvironmental Engineering, 2004, 130(3): 274−283